HHS Public Access

Author manuscript

*Small*. Author manuscript; available in PMC 2016 February 04.

Published in final edited form as:

*Small*. 2015 February 4; 11(5): 597–603. doi:10.1002/smll.201402230.

# Programmed Synthesis of Freestanding Graphene Nano-Membrane Arrays

**Pradeep Waduge**,
Department of Physics, Northeastern University, Boston, MA USA 02115

**Joseph Larkin**,
Department of Physics, Northeastern University, Boston, MA USA 02115

**Dr. Moneesh Upmanyu**,
Group of Simulation and Theory of Atomic-scale Material Phenomena (STAMP), Department of Mechanical and Industrial Engineering, Northeastern University, Boston, MA, USA 02115

**Dr. Swastik Kar**, and
Department of Physics, Northeastern University, Boston, MA USA 02115. Department of Physics, Northeastern University, Boston MA 02115, USA

**Dr. Meni Wanunu**
Department of Physics, Northeastern University, Boston, MA USA 02115. Department of Chemistry and Chemical Biology, Northeastern University, Boston, MA, USA. Department of Physics, Northeastern University, Boston MA 02115, USA

Pradeep Waduge: wanunu@neu.edu; Swastik Kar: s.kar@neu.edu

## Abstract

Freestanding graphene membranes are unique materials. The combination of atomically thin dimensions, remarkable mechanical robustness, and chemical stability, make porous and non-porous graphene membranes attractive for water purification and various sensing applications. Nanopores in graphene and other 2D materials have been identified as promising devices for next-generation DNA sequencing, based on readout of either transverse DNA base-gated current or through-pore ion current. While several ground breaking studies of graphene-based nanopores for DNA analysis have been reported, all methods reported to date require a physical transfer of the graphene from its source of production onto an aperture support. The transfer process is slow and often leads to tears in the graphene that render many devices useless for nanopore measurements. In this work, we report a novel scalable approach for site-directed fabrication of pinhole-free graphene nano-membranes. Our approach yields high quality few-layer graphene nano-membranes produced in less than a day using a few steps that do not involve transfer. We highlight the functionality of these graphene devices by measuring DNA translocation through electron-beam fabricated nanopores in such membranes.

Correspondence to: Swastik Kar, s.kar@neu.edu; Meni Wanunu.

Supporting Information

Supporting Information is available from the Wiley Online Library or from the author.

## Graphical Abstract

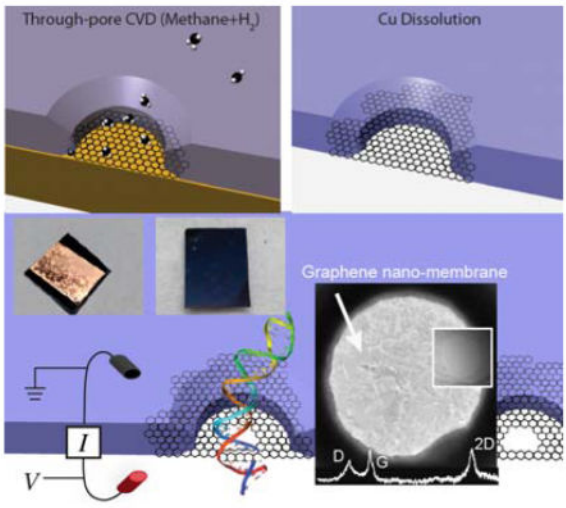


### Keywords

transfer-free graphene; nano-membranes; arrays; MEMS; nanopores

## 1. Introduction

Freestanding ultrathin membranes have attracted a lot of interest in recent years as filtration materials,[1–8] synthetic analogues of biological membranes,[9] and as MEMS-based sensor devices[10–13]. Ultrathin membranes have also found use as substrates for high-resolution nanopores, where the nanopores are tools for single-molecule detection and next-generation DNA sequencing.[14–17] While dielectrics such as silicon nitride (SiN),[18] aluminum oxide,[19, 20] and silicon oxide,[21] were thoroughly explored as membrane materials, there is a practical lower limit on membrane thickness for silicon-based membranes (~5–10 nm)[22–24] because silicon oxide and SiN are structurally and chemically more susceptible to damage during[25, 26] and after[27] pore fabrication. Since high-resolution readout of DNA requires robust ultrathin (<2 nm) membranes, other membrane materials have been explored such as graphene[28–30], boron nitride[31], DNA origami[32–34], hafnium oxide,[35, 36] and molybdenum disulphide ($MoS_2$)[37]. Due to its atomic thickness, mechanical properties, and unique electrical properties,[38–43] graphene in particular allows an additional sensing modality that may allow faster readout speeds and improved resolution. Finally, graphene membranes and their derivatives are impermeable to small molecules and ions, which allows pores in such membranes to be tailored for water desalination/purification[44] and selective molecular sieving[3, 45, 46].

Graphene can be obtained by mechanical exfoliation from graphite flakes[47, 48], chemical oxidation/reduction[49], chemical vapor deposition (CVD),[50] and epitaxial growth[51]. In this context, CVD-assisted graphene growth on appropriate catalytic metal surfaces has garnered considerable interest due to its relative ease of synthesis, low cost of production of large-area high-quality graphene, and lack of intense mechanical and chemical treatments.

While various approaches for graphene membranes have been reported for nanopore-based DNA analysis,[28–30, 52] these approaches require graphene transfer to an appropriately perforated substrate. Although considerable progress has been made in graphene transfer techniques,[30, 53–55] no process offers a scalable approach to produce a large number of membranes for use in nanopore and other membrane-related experiments. In addition, graphene membranes produced by "*synthesize-then-transfer-graphene*" protocols[30] can degrade the quality of the membranes by introducing wrinkles, cracks, and contamination during the transfer process. Recently, freestanding graphene membranes have been produced on TEM grids by a transfer-free approach on larger (~30μm) apertures,[56] although the ionic permeability of these membranes were not studied.

In this paper, we present a novel approach to fabricate *in-situ*, large arrays of few-layer freestanding pinhole-free graphene membranes. Few-layer graphene membranes are grown directly onto an array of sub-micrometer apertures in a scalable method. The graphene membranes grow precisely above the apertures to yield pinhole-free membranes, as determined by ionic current measurements. Since our method does not involve graphene transfer following its synthesis, this approach is more practical for obtaining freestanding graphene membranes with high yield.

## 2. Results and Discussion

### Graphene nano-membrane fabrication

The concept of our membrane fabrication, as well as a scheme of our five-step approach is shown in Figure 1. A typical process is outlined here: First, an array of 5 × 5 $mm^2$ silicon chips, each containing a freestanding low-stress SiN window (~40–80 μm), was cleaned in hot piranha and then rinsed copiously in warm deionized (DI) water, and then dried with a gentle flow of nitrogen ($N_2$) gas. Next, positive electron-beam resist was spun on the chips, and a 2×2 $μm^2$ portion of the SiN window was irradiated using e-beam lithography such that a pattern of five sub-micron holes was written and subsequently developed. Sub-micron holes through the nitride membrane were then generated by controlled etching using an $SF_6$ reactive ion etch (RIE) plasma. Resist was then stripped using acetone and a hot piranha treatment (Step 1). The chips were then placed in an atomic-layer deposition (ALD) instrument (Arradiance Gemstar) and a 10 nm thick $HfO_2$ film was deposited on both sides of the chip to passivate the SiN membrane (Step 2). This step was necessary as we found that subsequent graphene growth on unpassivated substrates resulted in contamination with silicon-based crystallites during the CVD process. After passivation, a ~200-nm-thick Cu film was deposited on the bottom of the membrane using thermal evaporation (Step 3). Graphene was then directly grown onto the Cu film over nano-apertures on SiN window using CVD at 1000°C using $CH_4$ and $H_2$ gases (Step 4). Following CVD the Cu catalyst was dissolved using 10% ammonium persulfate, and the device was rinsed with DI water and isopropanol (Step 5). Finally, nanopores were drilled through the graphene membranes using TEM.

### 2.1 Graphene nano-membrane characterization

Figure 2a shows a back-illuminated optical microscopy image of a low-stress freestanding SiN membrane with five nano-holes fabricated using e-beam lithography. Deposition of Cu on the membrane results in a layer of Cu catalyst on one side of the hole array. Figure 2b shows a back-illuminated optical image of the same membrane after 3-hour CVD graphene growth, following Cu dissolution. While the holes appear to be transparent, they are indeed covered with graphene: this is illustrated by comparative TEM images before (Figure 2c) and after (Figure 2d, Figure 2e) CVD-assisted graphene growth. In Figure 2c, which shows the nano-holes passivated with a thin film of $HfO_2$, holes are clearly present. The black rings observed around the nano-holes are due to a high contrast from the $HfO_2$ layer inside the holes. However, following graphene growth the nano-holes are all covered with freestanding graphene membranes. In Figure 2e, it is clear that some unetched nanoscopic Cu domains remain even after thorough the dissolution treatment using ammonium persulfate, probably due to its trapping between different graphene layers (see Supporting Information, Section S2). The contrasting patches seen in Figure 2e correspond to thickness variations in the CVD-grown graphene as the graphene flakes themselves are comprised of different number of graphene layers localized on the membrane. The few-layer graphene flakes are thin enough for rapid (5–10 seconds) nanopore fabrication using a highly focused electron beam of a TEM, noticeably faster than the typical time for drilling similar nanopores in conventional SiN membranes using similar conditions.[57] Several nanopores in the diameter range of 3–9 nm fabricated in different graphene devices are shown in Figure 2f. Raman spectra, which are typically used to characterize the thickness and quality of graphene,[58, 59] are shown in Figure 2g. The three curves shown represent spectra collected from the area of the nano-hole arrays in three different devices (though the laser beam could not be restricted to solely within the hole area). Pronounced 2D, G, and a weaker D band, are observed at ~2720, ~1582, and ~1360 $cm^{-1}$, respectively. It is well known that the quality and uniformity of CVD graphene is characterized by the $I_{2D}/I_G$ ratio, the peak positions of the 2D and G bands, and the full-width at half-maximum (FWHM) of the 2D band based on single-Lorentzian least squares fits.[50, 60, 61] In particular, the $I_{2D}/I_G$ ratio decreases as the number of graphene layers increases. Peak positions of G and 2D bands, the $I_{2D}/I_G$ ratio and FWHMs of 2D bands of the Raman spectra of three devices that we tested here confirm the formation of multilayer graphene (see Supporting Information, Section S1).[62] The presence of a weak D-band with CVD-assisted grown graphene is expected because the laser spot (~1 μm) is much larger than the size of a typical graphene domain (20–100 nm).

### 2.2 Ionic conductance measurements

The ionic conductance of transfer-free freestanding graphene membranes were studied by mounting graphene nano-membrane devices into a custom-made CTFE holder that allows 1M KCl electrolyte solution to be placed on either side of the membrane. Ag/AgCl electrodes immersed in each electrolyte bath were used to apply voltage in the range of ±300 mV across the membrane, and ion currents were measured using an Axopatch 200B patch-clamp amplifier. A current-voltage curve for a typical graphene nano-membrane device without a nanopore (red curve), as well as for a 7.5 nm (black curve) and a 20 nm (blue curve) diameter pore are shown in Figure 3. First, the mean conductance of bare graphene nano-membranes was in the range of 100–500 pS, as measured from the slopes of the

current-voltage curves for ten separate devices (four of them shown in inset to Figure 3). Such low conductance values, on par with monolayer graphene membranes,[28] corresponds to an extremely low pinhole fraction in the membrane. Of 50 devices tested over the course of the project, only 20% exhibited leakage that would correspond to unintentional holes and tears. In contrast to the pristine devices, the ion conductance of the 7.5 nm and 20 nm diameter pores is much greater due to ion transport through the pore orifice. For an infinitely thin insulating membrane with a circular pore of diameter *d*, the ionic conductance *G* through the pore is defined as:[63]

$$G=\sigma d \quad (1)$$

where σ =0.096 S/cm is the measured specific conductance of buffer at 25°C. The calculated *G* values for transfer-free graphene membranes from known $\sigma$ and *d*, indicated in Figure 3, yield *d* values of 2.5 nm and 6.7 nm for the 7.5 and 20 nm pores, respectively. This 3-fold discrepancy between TEM-based and measured diameters becomes clear when we present our investigation of DNA translocation through these pores in the next section.

### 2.3 Noise Characteristics

The noise characteristics of ion current signals through pores have been studied profusely. Uncoated graphene nanopores exhibit a high noise as compared with silicon nitride and other hydrophilic pores in inorganic dielectrics. In the inset to Figure 3 we present noise power spectral density (PSD) plots for a ~7.5 nm diameter graphene pore at 0 mV and 200 mV. We find that despite a similar PSD for our transfer-free graphene nano-membrane to that of a transferred graphene membrane with a similar diameter pore,[29] the *1/f* noise increases drastically and dominates the noise upon application of a 200 mV bias. We attribute this increase in *1/f* noise to the poor surface characteristics of the unmodified graphene surface, i.e., hydrophobic patches[64] and mechanically unstable pore edges. While coating the pores, i.e., with an ALD film of $TiO_2$[29] or $Al_2O_3$[65], improves the noise drastically, herein we report the properties of the bare untreated graphene surface. Finally, we note that in all reported measurements we did not include ~30% of devices which showed a complete current overload (>1,000 nS), possibly due to a crack through the membrane during fabrication or handling during device assembly.

### 2.4 Double-Stranded DNA Transport

In Figure 4a we show a characteristic continuous 20-second raw current trace of a 7.5 nm pore at 300 mV voltage upon the addition of linear 2,000 bp dsDNA to a final concentration of 8 nM into the negatively biased *cis* chamber. The stochastic appearance of downward spikes corresponds to interactions with individual DNA molecules with the pore. Analysis of the pulse characteristics was carried out using OpenNanopore open-source software developed by the Radenovic group.[66] The program uses a cumulative sum algorithm to identify and measure the dwell time ($t_d$) and current blockade amplitude ($\Delta I$) for each spike. The inset to Figure 4a shows example pulses retrieved from the analysis.

Scatter plots of $\Delta I$ vs. $t_d$ for 225 mV and 300 mV are shown in Figure 4b. The plot shows a distribution of dwell times for 225 mV that is much broader and longer than observed for

DNA transport through similar-diameter pores in silicon nitride, for example.[67] In comparison with other graphene pores, the mean $t_d$ value we have observed for 2 kbp dsDNA through our 7.5 nm diameter graphene nanopore at 225 mV translate to mean velocities that are ~ 3 times slower than observed for transport of 15 kbp dsDNA through a nanopore in transferred-few-layer graphene at 100 mV.[29] A closer inspection of the dwell time distributions for our experiments reveals two distinct populations that are resolvable in terms of dwell times, which we attribute to brief DNA collisions and full DNA translocations through the pore. The broad nature of the translocation population at 225 mV, which ranges from 0.5 – 10 ms, is possibly a result of sticky interactions of the DNA with the pore due to the hydrophobic surface characteristics of graphene. Increasing the voltage to 300 mV increases the force applied to the DNA molecules, which shifts the translocation time distribution to faster dwell times in range 80–500 μs while greatly reducing the scatter.

Analysis of the most probable dwell time populations ($t_d$) at four voltages in the range 225 – 300 mV is shown in Figure 4c (see Supporting Information Figure S1 for details). Peak $t_d$ values decrease exponentially with increasing voltage, while collision times are independent of the applied bias voltage in the range 225–300 mV. The regular decrease in the spread of $t_d$ values, along with the exponential decrease in peak $t_d$ values with increasing voltage, points to a transition from diffusion-dominated transport at low bias values to drift-dominated transport at higher bias values, and suggests that interactions of DNA with bare graphene significantly impact its transport behavior.

Finally, histograms of $\Delta I$ at each DNA translocation experimental voltage are shown in Figure 4d. We observe that current blockades increase linearly with voltage in the range 225–300 mV, while the fractional blockade values, i.e., $<\Delta I>/I_o$, are constant in this range. This suggests that the nanopore size does not change during the course of the experiment and/or at different voltages. Based on the open pore current ($I_o$) values and mean $\Delta I$ values, calculation of the effective pore diameter $d$ and effective thickness $h_{eff}$ of our graphene pores yields $d$ = 6.5 nm and $h_{eff}$ = 8 nm. Earlier in the paper we have noted that in the limit of infinitely thin nanopores, our calculated $G$ values based on TEM measurements deviate by three-fold from measured values of $G$. Using the information from DNA translocation experiments, we have now established that our graphene pores are indeed thicker than the infinitely thin limit (i.e., single-layer graphene), hence resolving this discrepancy between calculated and experimental $d$ values. This relatively thick value is most likely due to the growth conditions, which can be optimized in future experiments by fine-tuning the graphene growth parameters.

## 3. Conclusions

We have developed a scalable, few-step, transfer-free method for fabricating *in-situ* freestanding graphene membranes over nanoscale holes in thin solid-state membranes. The main highlight of our approach is that it does not require the low-throughput physical transfer of graphene material from its source of production to a freestanding membrane, a time-consuming process that often leads to cracks and tears in the graphene sheet, in addition to residual contamination from polymer supports used in the transfer process (e.g., PMMA). Moreover, since all steps in our fabrication process are scalable, the method

enables the production of freestanding graphene membranes over a whole wafer. We have shown that our graphene nano-membranes are free of pinholes, robust, and nanopores in such membranes exhibit similar ion transport characteristics as reported devices that utilize transferred graphene. In addition, we find that the ion current noise properties increase significantly with applied voltage, suggesting that the graphene surface needs to be modified to a more hydrophilic state in order to reduce hydrophobic pockets that dominate the noise. DNA translocation through nanopores in our graphene nano-membranes demonstrates the mechanical robustness of our devices, as the nanopores show long time stability and similar behavior over time. The high yield of devices without pinholes and cracks, which stands at 60–70%, makes the devices practical for experiments. However, we have noted that our process has yielded relatively thick pores. We hope that growth parameters can be tuned in future studies to obtain more 2D-like membranes. Finally, due to the nature of the CVD growth process, other 2D materials such as $MoS_2$ and BN should be compatible with our approach. Therefore, we strongly believe that the novel fabrication technique we developed to produce transfer-free freestanding graphene membranes will pave the way for large-scale fabrication of graphene and other 2D material-based membranes.

## 4. Experimental Section

Substrates for nanopore fabrication were 5×5 $mm^2$ Si chips with a 100-nm-thick SiN film deposited on a 2.5-μm-thick thermal $SiO_2$ layer, which helps to reduce electrical noise. SiN was protected with a 950 PMMA etch mask, and a small region (2×2 $\mu m^2$ square region with a pattern of four 450 nm-diameter holes and a central 800 nm hole) was exposed using Nabity NPGS e-beam writing software on a Hitachi S-4800 scanning electron microscope. Exposed PMMA was developed with 3:1 isopropyl alcohol and methyl isobutylketone, and AFM- and ellipsometry-calibrated thicknesses of SiN were etched in a Technics Micro-RIE Series 800 etcher using sulfur hexafluoride ($SF_6$) at 300 mTorr and 150 W. PMMA was removed using 30 min treatment with acetone and chips were cleaned with hot piranha followed by warm water to remove the residual PMMA. $HfO_2$ films were deposited at 150°C using a benchtop ALD system (Arradiance Gemstar), with tetrakis(ethylmethylamino) hafnium and $H_2O$ used as a precursor and oxidizer, respectively. A calibrated thickness of Cu was evaporated on the membrane side of the chip using a vacuum thermal evaporation system. Graphene membranes were synthesized using a low-pressure CVD technique in a split tube furnace with a 35 mm O.D. quartz tube as follows: Following Cu deposition, the chips were placed in the center of the furnace and the vacuum system was turned on. Once the pressure inside the furnace became ~ 11 mTorr, 35 sccm of $H_2$ were allowed to flow and the tube was heated to growth temperature of 1000°C. Upon reaching 1000°C the $H_2$ flow rate was reduced to 2 sccm, and 35 sccm of $CH_4$ gas were flowed for 3 h for graphene growth. During the growth process, the vacuum of the whole system was kept under 1.5 Torr. Following deposition, the furnace was allowed to naturally cool down to room temperature under a 35 sccm flow of $H_2$. After removal of the chips from the furnace the Cu was etched using 10% ammonium persulfate, and then the chips were rinsed with DI water and isopropyl alcohol and dried under a gentle flow of dry $N_2$. Raman spectroscopy was carried out using a Jobin Yvon LabRam HR800 spectrometer attached to an Olympus BH2 microscope. Graphene nanopores were fabricated and imaged at

Northeastern University using a JEOL 2010FEG transmission electron microscope operating in bright-field mode at 200 kV.

## Supplementary Material

Refer to Web version on PubMed Central for supplementary material.

## Acknowledgments

E. Panaitescu and L. Menon are gratefully acknowledged for allowing the use of the thermal evaporation system, and F. Liu for assistance with CVD and Raman Spectroscopy. The project was supported by a Northeastern University seed grant, as well as partial support from National Institutes of Health (R21-HG006873, MW) and National Science Foundation (ECCS 1351424, SK).

## References

1. Berry V. Carbon. 2013; 62:1–10.
2. Kim HW, Yoon HW, Yoon SM, Yoo BM, Ahn BK, Cho YH, Shin HJ, Yang H, Paik U, Kwon S. Science. 2013; 342(6154):91–95. [PubMed: 24092738]
3. Nair R, Wu H, Jayaram P, Grigorieva I, Geim A. Science. 2012; 335(6067):442–444. [PubMed: 22282806]
4. Hauser AW, Schwerdtfeger P. J Phys Chem Lett. 2012; 3(2):209–213.
5. Drahushuk LW, Strano MS. Langmuir. 2012; 28(48):16671–16678. [PubMed: 23101879]
6. Jiang DE, Cooper VR, Dai S. Nano Lett. 2009; 9(12):4019–4024. [PubMed: 19995080]
7. O'Hern SC, Stewart CA, Boutilier MS, Idrobo JC, Bhaviripudi S, Das SK, Kong J, Laoui T, Atieh M, Karnik R. ACS Nano. 2012; 6(11):10130–10138. [PubMed: 23030691]
8. Du H, Li J, Zhang J, Su G, Li X, Zhao Y. The Journal of Physical Chemistry C. 2011; 115(47): 23261–23266.
9. Connelly LS, Meckes B, Larkin J, Gillman AL, Wanunu M, Lal R. ACS App Mat Int. 2014; 6(7): 5290–5296.
10. Smith AD, Niklaus F, Paussa A, Vaziri S, Fischer AC, Sterner M, Forsberg F, Delin A, Esseni D, Palestri P. Nano Lett. 2013; 13(7):3237–3242. [PubMed: 23786215]
11. Liao M, Koide Y. Critical Reviews in Solid State and Materials Sciences. 2011; 36(2):66–101.
12. Basu S, Bhattacharyya P. Sensors and Actuators B: Chemical. 2012; 173:1–21.
13. Miao T, Yeom S, Wang P, Standley B, Bockrath M. Nano Lett. 201410.1021/nl403936a
14. Saha KK, Drndic M, Nikolic BK. Nano Lett. 2012; 12(1):50–55.10.1021/nl202870y [PubMed: 22141739]
15. Puster M, Rodriguez-Manzo JA, Balan A, Drndic M. ACS Nano. 2013; 7(12):11283–11289.10.1021/nn405112m [PubMed: 24224888]
16. Wilson J, Di Ventra M. Nanotechnology. 2013; 24(41):415101.10.1088/0957-4484/24/41/415101 [PubMed: 24061386]
17. Traversi F, Raillon C, Benameur SM, Liu K, Khlybov S, Tosun M, Krasnozhon D, Kis A, Radenovic A. Nat Nanotechnol. 2013; 8(12):939–945.10.1038/nnano.2013.240 [PubMed: 24240429]
18. Aziz M, Golovchenko J, Branton D, McMullan C, Stein D, Li J. Nature. 2001; 412(6843):166–169. [PubMed: 11449268]
19. Chen P, Mitsui T, Farmer DB, Golovchenko J, Gordon RG, Branton D. Nano Lett. 2004; 4(7): 1333–1337. [PubMed: 24991194]
20. Venkatesan BM, Dorvel B, Yemenicioglu S, Watkins N, Petrov I, Bashir R. Adv Mater. 2009; 21(27):2771–2776.10.1002/adma.200803786 [PubMed: 20098720]
21. Storm AJ, Chen JH, Ling XS, Zandbergen HW, Dekker C. Nat Mater. 2003; 2(8):537–540.10.1038/Nmat941 [PubMed: 12858166]

22. Wanunu M, Dadosh T, Ray V, Jin J, McReynolds L, Drndić M. Nat Nanotechnol. 2010; 5(11): 807–814. [PubMed: 20972437]
23. Kuan AT, Golovchenko JA. Applied Physics Letters. 2012; 100(21):213104–213104-4. [PubMed: 22711913]
24. Niedzwiecki DJ, Iyer R, Borer PN, Movileanu L. ACS Nano. 2013; 7(4):3341–3350.10.1021/Nn400125c [PubMed: 23445080]
25. Liebes Y, Hadad B, Ashkenasy N. Nanotechnology. 2011; 22(28):285303. [PubMed: 21636881]
26. Wu M-Y, Krapf D, Zandbergen M, Zandbergen H, Batson PE. Applied Physics Letters. 2005; 87:113106.
27. van den Hout M, Hall AR, Wu MY, Zandbergen HW, Dekker C, Dekker NH. Nanotechnology. 2010; 21(11) Artn 115304. 10.1088/0957-4484/21/11/115304
28. Garaj S, Hubbard W, Reina A, Kong J, Branton D, Golovchenko J. Nature. 2010; 467(7312):190–193. [PubMed: 20720538]
29. Merchant CA, Healy K, Wanunu M, Ray V, Peterman N, Bartel J, Fischbein MD, Venta K, Luo ZT, Johnson ATC, Drndic M. Nano Lett. 2010; 10(8):2915–2921.10.1021/Nl101046t [PubMed: 20698604]
30. Schneider GF, Kowalczyk SW, Calado VE, Pandraud G, Zandbergen HW, Vandersypen LMK, Dekker C. Nano Lett. 2010; 10(8):3163–3167.10.1021/Nl102069z [PubMed: 20608744]
31. Liu S, Lu B, Zhao Q, Li J, Gao T, Chen YB, Zhang YF, Liu ZF, Fan ZC, Yang FH, You LP, Yu DP. Adv Mater. 2013; 25(33):4549–4554.10.1002/adma.201301336 [PubMed: 23775629]
32. Wei R, Martin TG, Rant U, Dietz H. Angewandte Chemie. 2012; 124(20):4948–4951.
33. Langecker M, Arnaut V, Martin TG, List J, Renner S, Mayer M, Dietz H, Simmel FC. Science. 2012; 338(6109):932–936. [PubMed: 23161995]
34. Bell NA, Engst CR, Ablay M, Divitini G, Ducati C, Liedl T, Keyser UF. Nano Lett. 2011; 12(1): 512–517. [PubMed: 22196850]
35. Shim J, Rivera JA, Bashir R. Nanoscale. 2013; 5(22):10887–10893.10.1039/C3NR02608F [PubMed: 23945603]
36. Larkin J, Henley R, Bell DC, Cohen-Karni T, Rosenstein JK, Wanunu M. ACS Nano. 2013; 7(11): 10121–10128. [PubMed: 24083444]
37. Liu K, Feng JD, Kis A, Radenovic A. ACS Nano. 2014; 8(3):2504–2511.10.1021/nn406102h [PubMed: 24547924]
38. Booth TJ, Blake P, Nair RR, Jiang D, Hill EW, Bangert U, Bleloch A, Gass M, Novoselov KS, Katsnelson MI, Geim AK. Nano Lett. 2008; 8(8):2442–2446.10.1021/nl801412y [PubMed: 18593201]
39. Geim A. Nature. 2005; 438(7065):197–200. [PubMed: 16281030]
40. Geim AK. Science. 2009; 324(5934):1530–1534. [PubMed: 19541989]
41. Lee C, Wei X, Kysar JW, Hone J. Science. 2008; 321(5887):385–388. [PubMed: 18635798]
42. Wang X, Zhi L, Müllen K. Nano Lett. 2008; 8(1):323–327. [PubMed: 18069877]
43. Zhang Y, Tan YW, Stormer HL, Kim P. Nature. 2005; 438(7065):201–204. [PubMed: 16281031]
44. Wang EN, Karnik R. Nat Nanotechnol. 2012; 7(9):552–554. [PubMed: 22948936]
45. Koenig SP, Wang L, Pellegrino J, Bunch JS. Nat Nanotechnol. 2012; 7(11):728–732. [PubMed: 23042491]
46. Joshi R, Carbone P, Wang F, Kravets V, Su Y, Grigorieva I, Wu H, Geim A, Nair R. 2014 arXiv preprint arXiv:1401.3134.
47. Novoselov KS, Geim AK, Morozov S, Jiang D, Zhang Y, Dubonos S, Grigorieva I, Firsov A. Science. 2004; 306(5696):666–669. [PubMed: 15499015]
48. Novoselov K, Jiang D, Schedin F, Booth T, Khotkevich V, Morozov S, Geim A. Proceedings of the National Academy of Sciences of the United States of America. 2005; 102(30):10451–10453. [PubMed: 16027370]
49. Stankovich S, Dikin DA, Piner RD, Kohlhaas KA, Kleinhammes A, Jia Y, Wu Y, Nguyen ST, Ruoff RS. Carbon. 2007; 45(7):1558–1565.

50. Li X, Cai W, An J, Kim S, Nah J, Yang D, Piner R, Velamakanni A, Jung I, Tutuc E. Science. 2009; 324(5932):1312–1314. [PubMed: 19423775]
51. Sutter P. Nat Mater. 2009; 8(3):171–172. [PubMed: 19229263]
52. Garaj S, Liu S, Golovchenko JA, Branton D. Proceedings of the National Academy of Sciences. 2013; 110(30):12192–12196.
53. Li XS, Zhu YW, Cai WW, Borysiak M, Han BY, Chen D, Piner RD, Colombo L, Ruoff RS. Nano Lett. 2009; 9(12):4359–4363.10.1021/nl902623y [PubMed: 19845330]
54. Liang X, Sperling BA, Calizo I, Cheng G, Hacker CA, Zhang Q, Obeng Y, Yan K, Peng H, Li Q. ACS Nano. 2011; 5(11):9144–9153. [PubMed: 21999646]
55. Lin WH, Chen TH, Chang JK, Taur JI, Lo YY, Lee WL, Chang CS, Su WB, Wu CI. ACS Nano. 2014; 8(2):1784–1791.10.1021/nn406170d [PubMed: 24471977]
56. Alemán B, Regan W, Aloni S, Altoe V, Alem N, Girit C, Geng B, Maserati L, Crommie M, Wang F. ACS Nano. 2010; 4(8):4762–4768. [PubMed: 20604526]
57. Kim MJ, Wanunu M, Bell DC, Meller A. Adv Mater. 2006; 18(23):3149–3155.10.1002/adma.200601191
58. Pimenta M, Dresselhaus G, Dresselhaus MS, Cancado L, Jorio A, Saito R. Phys Chem Chem Phys. 2007; 9(11):1276–1290. [PubMed: 17347700]
59. Ferrari AC. Solid State Commun. 2007; 143(1):47–57.
60. Ferrari A, Meyer J, Scardaci V, Casiraghi C, Lazzeri M, Mauri F, Piscanec S, Jiang D, Novoselov K, Roth S. Phys Rev Lett. 2006; 97(18):187401. [PubMed: 17155573]
61. Yan K, Peng H, Zhou Y, Li H, Liu Z. Nano Lett. 2011; 11(3):1106–1110. [PubMed: 21322597]
62. Hwang JS, Lin YH, Hwang JY, Chang R, Chattopadhyay S, Chen CJ, Chen P, Chiang HP, Tsai TR, Chen LC. Nanotechnology. 2013; 24(1):015702. [PubMed: 23221149]
63. Hall JE. J Gen Physiol. 1975; 66(4):531–532. [PubMed: 1181379]
64. Wang S, Zhang Y, Abidi N, Cabrales L. Langmuir. 2009; 25(18):11078–11081. [PubMed: 19735153]
65. Venkatesan BM, Estrada D, Banerjee S, Jin XZ, Dorgan VE, Bae MH, Aluru NR, Pop E, Bashir R. ACS Nano. 2012; 6(1):441–450.10.1021/Nn203769e [PubMed: 22165962]
66. Raillon C, Granjon P, Graf M, Steinbock LJ, Radenovic A. Nanoscale. 2012; 4(16):4916–4924.10.1039/C2nr30951c [PubMed: 22786690]
67. Wanunu M, Sutin J, McNally B, Chow A, Meller A. Biophys J. 2008; 95(10):4716–4725. [PubMed: 18708467]

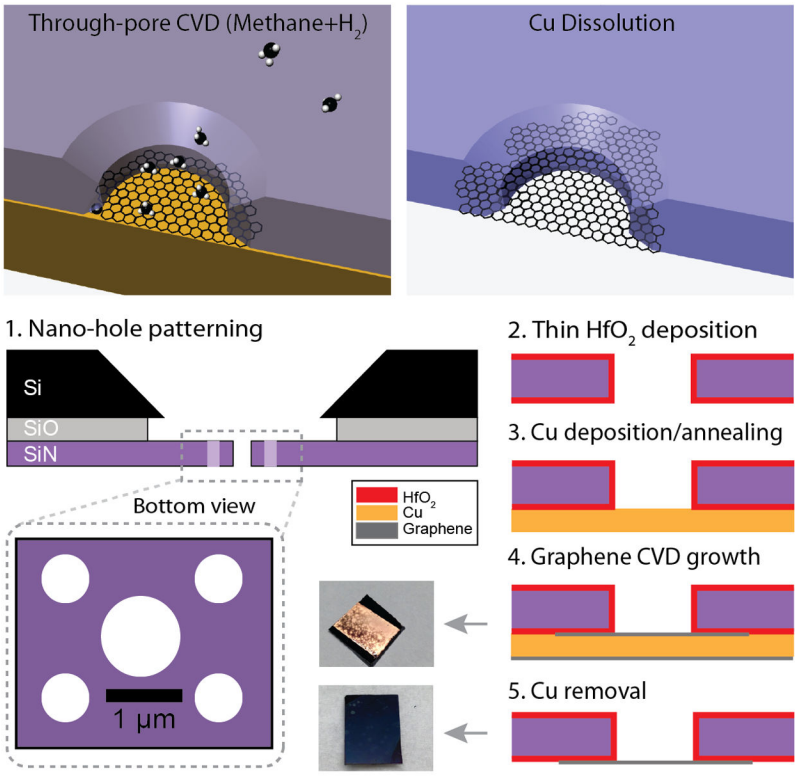


**Figure 1.**

Freestanding graphene nano-membrane fabrication. Top: Illustration of Cu-assisted graphene nano-membrane fabrication over a predefined nano-hole in a silicon nitride support membrane. Bottom: Side-view of a silicon nitride membrane during our five-step process that includes: 1) Hole array formation using e-beam lithography and reactive-ion etching, 2) Atomic-layer deposition of a 10-nm-thick $HfO_2$ passivation layer on both sides of the membrane, 3) Cu deposition (thickness ~200 nm) onto the bottom side of the membrane by thermal evaporation. 4) Graphene growth using chemical vapor deposition (CVD), 5) Cu etching using 10% ammonium persulfate to release the suspended graphene nano-membrane. Optical images of the chips following steps 4 and 5 are shown to the left of the corresponding steps. Note that in steps 2–5 only one of the five nano-holes is shown.

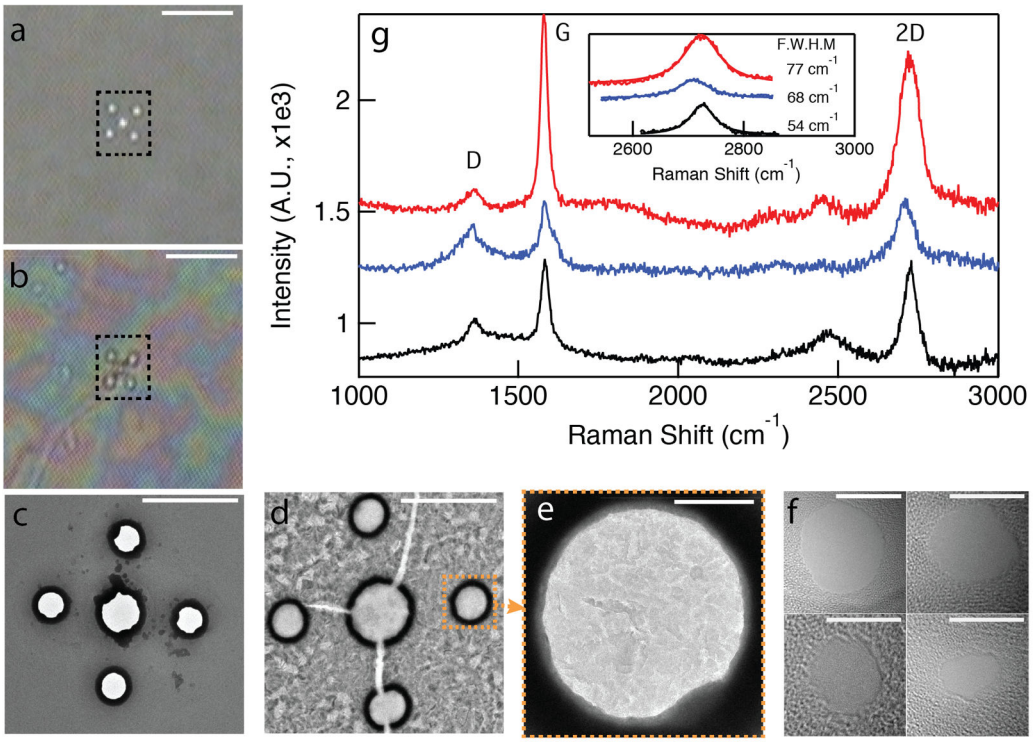


**Figure 2.**

Freestanding graphene nano-membrane characterization. a) Back-illuminated optical image of a low-stress freestanding SiN membrane with four sub-micron diameter holes (dashed box) before CVD-assisted graphene growth (scale bar = 20 μm). b) Optical image of the same membrane after graphene growth and Cu removal (scale bar = 20 μm). c) Bright-field (BF) TEM image of the nano-hole array following ALD deposition of $HfO_2$, prior to graphene growth (scale bar = 2 μm). d) BF-TEM image of the same membrane after CVD-assisted graphene growth and Cu removal (scale bar = 2 μm). e) Zoomed-in TEM image of one of the five nano-holes, revealing graphene nano-domains of varying contrast, i.e., thickness (scale bar = 100 nm). f) BF-TEM images of representative nanopores fabricated in the freestanding nano-membranes (scale bars = 5 nm). g) Raman spectra of three different graphene membrane devices, collected from areas that contain the nano-hole arrays. Inset shows FWHM values of the 2D-peaks from single-Lorentzian fits (66±12 $cm^{-1}$), which indicate a multi-layer graphene structure.

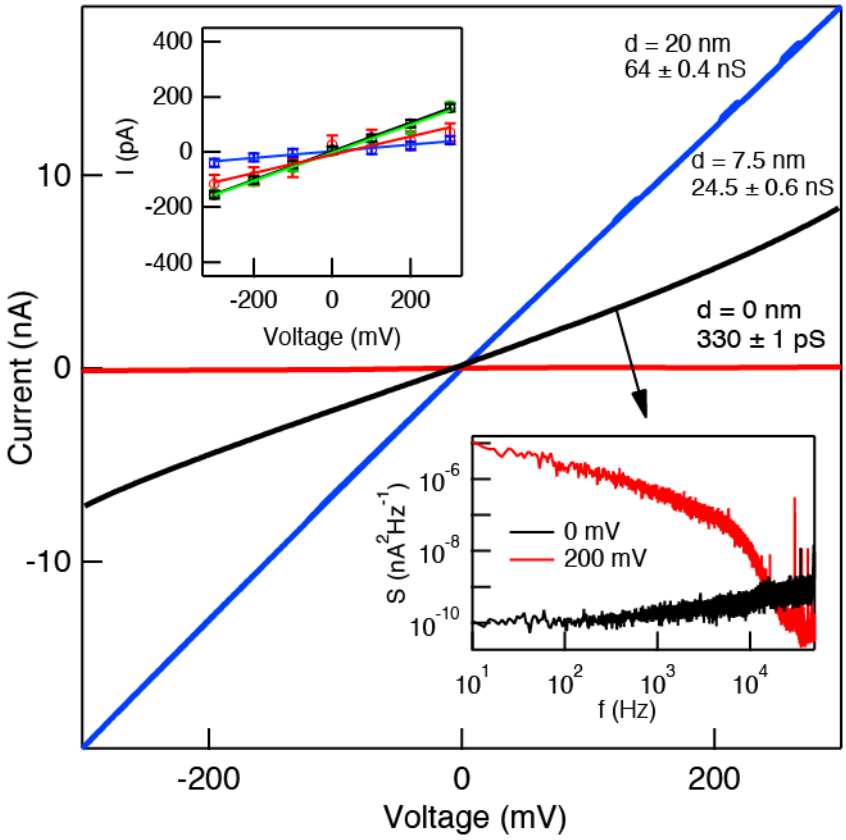


**Figure 3.**

Ionic conductance of graphene nanopores. Typical current-voltage curves of graphene nano-membrane (red), and for *d* = 7.5 nm (black), and *d* = 20 nm (blue) pores. Conductance values for these curves are indicated in the figure. Top inset: current-voltage curves for four different graphene nano-membrane devices without pores. Bottom inset: noise power spectral densities (PSD) for the ~7.5 nm diameter graphene pore at 0 mV and 200 mV applied voltage (sampling rate = 250 kHz, low-pass filtered at 10 kHz, T = 25°C, 1 M KCl, pH 8.3).

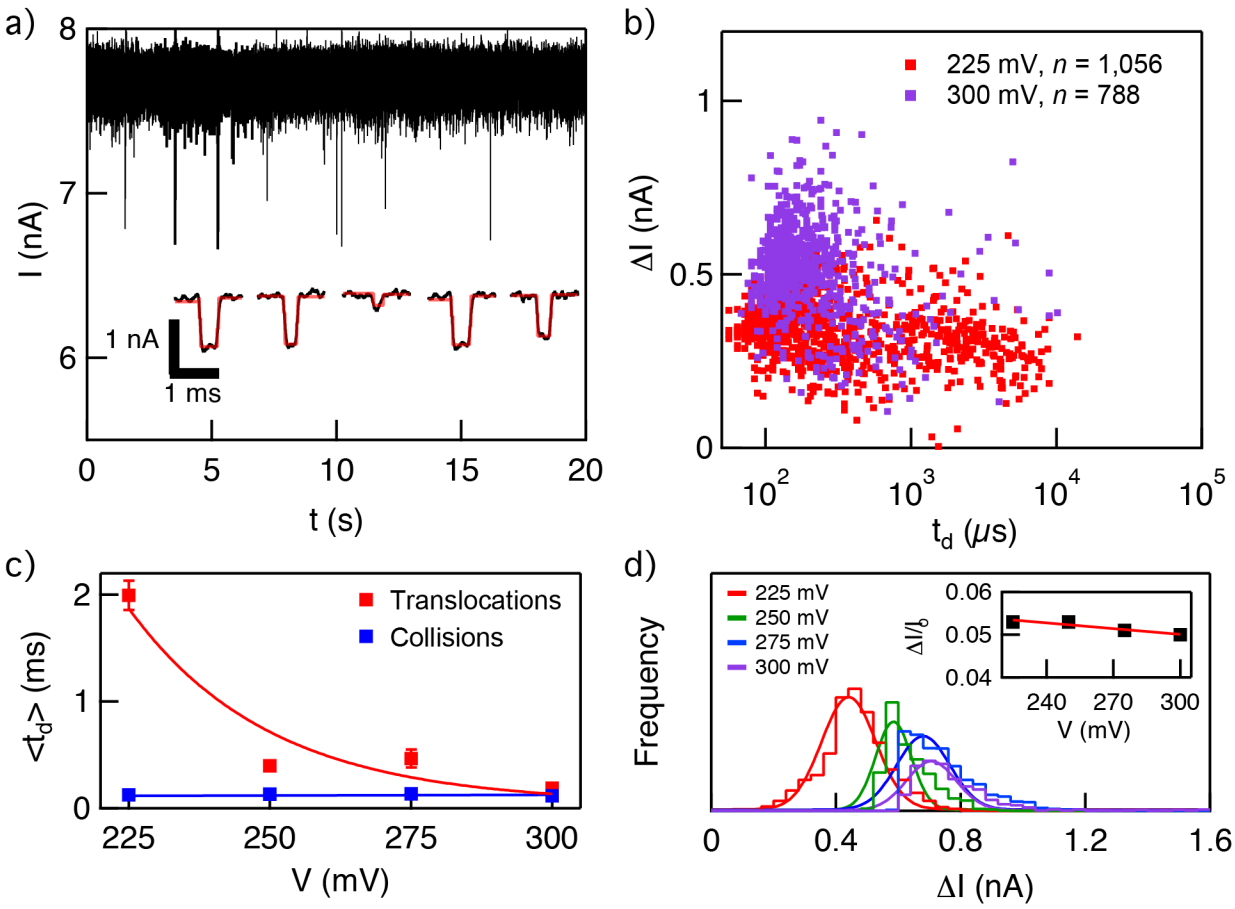


**Figure 4.**

Double-stranded DNA transport through a graphene nanopore. a) Continuous ~20-second long current vs. time trace of 7.5 nm pore at 300 mV applied voltage after the addition of 8 nM linear 2,000 bp to the *cis* chamber. Downward spikes correspond to DNA interactions with the pore. Inset shows a magnified view of representative events, extracted from the trace following analysis using OpenNanopore software (fit shown as red curve). b) Scatter plot of Δ*I vs.* $t_d$ at 225 mV and 300 mV (n=1,056 and n=788, respectively). c) Mean $t_d$ values as a function of voltage, which correspond to translocation and collision timescales (see Supporting Information Figure S1 for details). d) Histograms of Δ*I* at different voltages in the range 225–300 mV. Inset shows the fractional current $\Delta I/I_o$, which remains constant in the tested voltage range.